Toward controllable Si-doping in oxide molecular beam epitaxy using a solid SiO source: Application to β-Ga$_2$O$_3$ (EP)

(iD) A. Ardenghi, (iD) O. Bierwagen, (iD) A. Falkenstein, et al.

COLLECTIONS

Paper published as part of the special topic on Wide- and Ultrawide-Bandgap Electronic Semiconductor Devices

EP   This paper was selected as an Editor's Pick

ARTICLES YOU MAY BE INTERESTED IN

β-Ga$_2$O$_3$ FinFETs with ultra-low hysteresis by plasma-free metal-assisted chemical etching
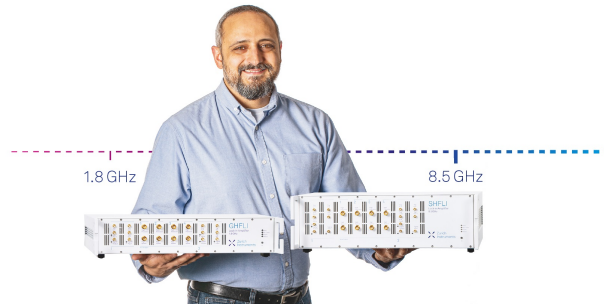Applied Physics Letters **121**, 052102 (2022); https://doi.org/10.1063/5.0096490

Electron mobility in ordered β–(Al$_x$Ga$_{1-x}$)$_2$O$_3$ alloys from first-principles
Applied Physics Letters **121**, 042103 (2022); https://doi.org/10.1063/5.0096341

An energy conserving mechanism for temporal metasurfaces
Applied Physics Letters **121**, 041702 (2022); https://doi.org/10.1063/5.0097591

Toward controllable Si-doping in oxide molecular beam epitaxy using a solid SiO source: Application to β-Ga$_2$O$_3$ ᴇᴘ

View Online   Export Citation   CrossMark

A. Ardenghi,[1,a] ᴵᴰ O. Bierwagen,[1,a] ᴵᴰ A. Falkenstein,[2] ᴵᴰ G. Hoffmann,[1] ᴵᴰ J. Lähnemann,[1] ᴵᴰ M. Martin,[2] ᴵᴰ and P. Mazzolini[3,a] ᴵᴰ

AFFILIATIONS

[1]Paul-Drude-Institut für Festkörperelektronik, Leibniz-Institut im Forschungsverbund Berlin e.V., Hausvogteiplatz 5-7, 10117 Berlin, Germany
[2]Institute of Physical Chemistry, RWTH Aachen University, D-52056 Aachen, Germany
[3]Department of Mathematical, Physical, and Computer Sciences, University of Parma, Parco Area delle Scienze 7/A, 43124, Parma, Italy

Note: This paper is part of the APL Special Collection on Wide- and Ultrawide-Bandgap Electronic Semiconductor Devices.
[a]Authors to whom correspondence should be addressed: ardenghi@pdi-berlin.de; bierwagen@pdi-berlin.de; and piero.mazzolini@unipr.it

ABSTRACT

The oxidation-related issues in controlling Si doping from the Si source material in oxide molecular beam epitaxy (MBE) are addressed by using its solid suboxide, SiO, as an alternative source material in a conventional effusion cell. Line-of-sight quadrupole mass spectrometry of the direct SiO-flux (Φ_{SiO}) from the source at different temperatures (T_{SiO}) confirmed SiO molecules to sublime with an activation energy of 3.3 eV. The T_{SiO}-dependent Φ_{SiO} was measured in vacuum before and after subjecting the source material to an O$_2$-background of 10^{-5} mbar (typical oxide MBE regime). The absence of a significant Φ_{SiO} difference indicates negligible source oxidation in molecular O$_2$. Mounted in an oxygen plasma-assisted MBE, Si-doped β-Ga$_2$O$_3$ layers were grown using this source. The Φ_{SiO} at the substrate was evaluated [from 2.9×10^9 cm^{-2} s^{-1} ($T_{SiO} = 700\,^\circ$C) to 5.5×10^{13} cm^{-2} s^{-1} ($T_{SiO} = 1000\,^\circ$C)] and Si-concentration in the β-Ga$_2$O$_3$ layers measured by secondary ion mass spectrometry highlighting unprecedented control of continuous Si-doping for oxide MBE, i.e., N_{Si} from 4×10^{17} cm^{-3} ($T_{SiO} = 700\,^\circ$C) up to 1.7×10^{20} cm^{-3} ($T_{SiO} = 900\,^\circ$C). For a homoepitaxial β-Ga$_2$O$_3$ layer, a Hall charge carrier concentration of 3×10^{19} cm^{-3} in line with the provided Φ_{SiO} ($T_{SiO} = 800\,^\circ$C) is demonstrated. No SiO-incorporation difference was found between β-Ga$_2$O$_3$(010) layers homoepitaxially grown at 750\,$^\circ$C and β-Ga$_2$O$_3$($-$201) heteroepitaxial layers grown at 550\,$^\circ$C on c-plane sapphire. However, the presence of activated oxygen (plasma) resulted in partial source oxidation and related decrease in doping concentration (particularly at $T_{SiO} < 800\,^\circ$C), which has been tentatively explained with a simple model. Degassing the source at 1100\,$^\circ$C reverted this oxidation. Concepts to reduce source oxidation during MBE-growth are referenced.

Due to a high variety of functional properties, metal oxides are rising in popularity as material systems for innovative optoelectronic devices.[1] Among metal oxides, monoclinic β-Ga$_2$O$_3$ is one of the most interesting ones, and it has been particularly intensely investigated in the past decade.[2] In fact, due to a predicted breakdown field around 8 MV/cm as a consequence of its bandgap of about 4.8 eV, β-Ga$_2$O$_3$ is one of the most promising novel materials for power electronics.[3] Moreover, it can be grown from the melt[4–7] in turn allowing for β-Ga$_2$O$_3$ homoepitaxy of high quality layers.[3]

To obtain a broad range of devices for power electronic application, a thorough control on the electrical properties is needed.[8] Considering the lack of p-type doping for Ga$_2$O$_3$,[9] the main focus is on the group-IV elements in order to tune n-type doping. So far, Ge, Si, and Sn have been already successfully employed as dopants in homoepitaxial layers grown with different technique, such as

molecular beam epitaxy (MBE),[5,10–15] Metal Organic Chemical Vapor Deposition (MOCVD),[16–19] and Metal Organic Vapor Phase Epitaxy (MOVPE).[20,21]

Lany has theoretically shown[22] that Si can be considered as a better donor compared to Ge and Sn, since it is predicted to be the only truly shallow donor among them. From a survey of experimental data collected on semiconducting homoepitaxial β-Ga$_2$O$_3$ layers,[8] the highest electron mobilities μ over a broad range of electron concentrations n are achieved with Si or Ge doping; the generally lower μ in Sn-doped films is likely related to a deep donor state identified for Sn.[12] Controlled Si doping in β-Ga$_2$O$_3$ has been already demonstrated in MOCVD but not in MBE. This is most likely linked to the two limitations of Si doping in MBE systems.

The first one is due to the unintentional incorporation of Si, probably related to the quartz cavity of the plasma source in oxygen plasma-assisted MBE (PAMBE)[23,24] and is limiting the low concentration side of the doping window ($N_{Si} < 10^{18}$ cm^{-3}).

The second one is due to instable Si-doping concentration in PAMBE-grown Ga$_2$O$_3$ layers that depend on the oxygen background pressure rather than the Si source temperature as pointed out by Kalarickal et al.[13] As an underlying process, they identified the oxidation of the elemental Si source resulting in the source flux to consist of the SiO suboxide, which has a higher vapor pressure than Si. Further oxidation of the Si surface into solid SiO$_2$ was identified by Krishnamoorthy et al.[15] to cause drastic flux reduction during layer growth due to the lower vapor pressure of SiO$_2$. Based on the underlying mechanisms, we conjecture ozone-MBE not to suffer from the first limitation but from the second one.

Indeed, the oxidation of the heated elemental source in an oxygen background into its volatile suboxide happens for many elements, including In, Ga, Ge, or Sn.[25] This suboxide formation at the source can determine the Ge- or Sn-doping of oxides (including in the Ga$_2$O$_3$ material system) or even the growth rates (GRs) for Ga$_2$O$_3$ during MBE deposition at relatively low Ga-source temperatures (e.g., <750 °C). Despite similar suboxide formation, the use of a Sn-metal source for Ga$_2$O$_3$ in PAMBE is more controllable with respect to a Si one[12] but can involve segregation problems.[26] For Ge-doping of Ga$_2$O$_3$ from a Ge-source in PAMBE, an additional strong dependence of doping concentration on the growth substrate temperature (T_g) has been shown.[14] High concentrations ($N_{Ge} \approx 10^{20}$ cm^{-3}) required relatively low T_g (600 °C), potentially placing limits on the crystal quality of the deposited layers.

An efficient solution to control Si doping in oxide MBE while avoiding massive oxidation of the source could be the use of an oxide or suboxide source material in the cell,[27] similar to the use of SnO$_2$, SnO, or mixtures of Sn and SnO$_2$ to produce a SnO flux,[26,28] or mixtures of Ga and Ga$_2$O$_3$ to produce a Ga$_2$O flux.[28,29] Major advantages in the use of a suboxide (or mixed elemental + oxide) sources over an oxide one are the significantly lower cell temperatures required and the absence of parasitic oxygen formation from the decomposition of the oxide source material.[28] On the contrary, controllable Si doping would benefit from a SiO$_2$ source that cannot oxidize further as SiO could. However, based on the vapor pressure of SiO$_2$,[27] the geometry of our growth chamber, and the temperature limit of conventionally employed effusion cells (1200 °C), the Si concentration in layers deposited at a typical growth rate of 4.5 nm/min would be limited to $N_{Si} \leq 10^{19}$ cm^{-3} for a SiO$_2$ source.

For example, a high-temperature effusion cell running at $T_{SiO_2} = 1400$ °C would be required to obtain $N_{Si} = 1 \times 10^{20}$ cm^{-3} [considering that a growth rate (GR) of 1 Å/s in our MBE system correlates with a partial pressure of the source material in the effusion cell on the order of 10^{-3} mbar (Ref. 28)].

In comparison, a SiO source could reach $N_{Si} = 1.7 \times 10^{20}$ cm^{-3} at $T_{SiO} = 900$ °C, which prompted us to characterize a solid SiO source for PAMBE growth with a focus on doping β-Ga$_2$O$_3$ layers. In particular, we demonstrate the possibility to obtain Si-doping concentrations on a wide range—from 4×10^{17} cm^{-3} (limited by the background Si concentration in the PAMBE deposited layers) up to 1.7×10^{20} cm^{-3}—in both homoepitaxial and heteroepitaxial β-Ga$_2$O$_3$ layers, with negligible dependence on the growth orientation and/or the growth temperature. For our study, an Al$_2$O$_3$ crucible loaded with 10 g of 3–6 mm SiO lumps (4 N purity, Alfa Aesar) was placed in a conventional single-filament effusion cell.

At first, we characterized the direct flux from this SiO source using a quadrupole mass spectrometer (QMS) mounted line in sight to the cell inside a custom-built system, which is schematically shown in the inset of Fig. 1 and described in Ref. 28. The composition of the flux from the SiO source at a base pressure in the low 10^{-8} mbar regime is reported in Fig. 1(a) for a cell temperature of $T_{SiO} = 1200$ °C chosen to maximize the signal-to-noise ratio for the identification of the different desorbing species. Due to the natural abundance of stable isotopes of Si at 28 amu (92.23%), 29 amu (4.67%), and 30 amu (3.1%), the major signals shown in Fig. 1(a) can be clearly identified as SiO. A weaker Si signal is recorded and related to fragmentation inside the QMS.[28] To remove interference with residual N$_2$ (having the same mass per charge as ^{28}Si), the measurements with closed cell shutter were subtracted from those with opened shutter. An Ar signal due to the background pressure is also visible. The same qualitative SiO spectra could be recorded down to $T_{SiO} = 880$ °C where the ^{44}SiO signal reaches the noise level.

To calculate the activation energy E_a for SiO sublimation, the ^{44}SiO signal was recorded at T_{SiO} ranging from 1200 to 800 °C in vacuum. The corresponding Arrhenius plot yields $E_a = 3.29$ eV [red line in Fig. 1(b)] in good agreement with the $E_a = 3.41$ eV [black line in Fig. 1(b)] extracted from the thermodynamic calculation of Adkison et al.[27]

To investigate potential source oxidation in molecular oxygen, the source was exposed to a controlled O$_2$ background of $p = 1 \times 10^{-5}$ mbar (typical for PAMBE growths) for periods of 30–180 min at various T_{SiO}. A potential surface oxidation to SiO$_2$ during this exposure is expected to reduce the SiO flux (Φ_{SiO}) with respect to the untreated SiO source material. Figure 2 shows the comparison of the measured SiO partial pressure during the ramp up (performed in vacuum) from $T_{SiO} = 700$ to 1200 °C before and after exposure of the source to an O$_2$ background pressure of 1×10^{-5} mbar for 3 h at $T_{SiO} = 700$ °C. The matching partial pressure recorded in both experiments indicates that the SiO source did not get oxidized. The initial (up to 15 min) higher values detected for the SiO partial pressure after the oxidation process (red dashed lines in Fig. 2) are due to the higher background pressure caused by residual oxygen in the chamber after the treatment and a limited mass filtering of the QMS.

Next, the crucible with the SiO source material was mounted in our PAMBE growth chamber for doping experiments. In order to predict the SiO-flux and consequential Si doping concentration in MBE deposited β-Ga$_2$O$_3$ layers as a function of the T_{SiO}, we extrapolated the

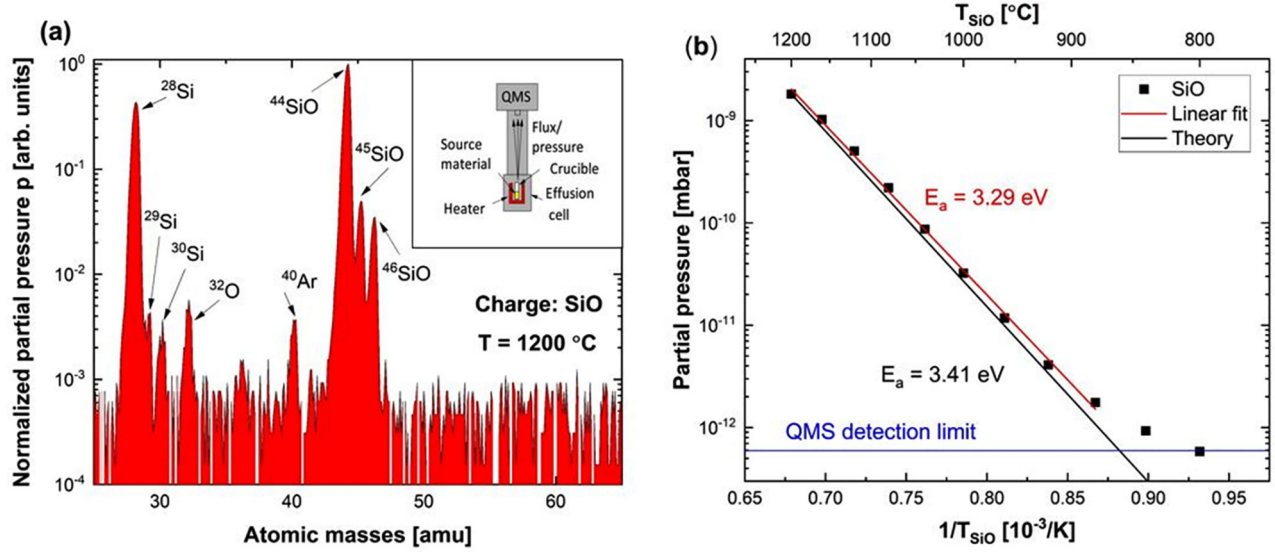**FIG. 1.** (a) QMS spectrum (red) of the flux from the SiO cell at $T_{SiO} = 1200\,°C$ in vacuum. Inset: sketch of the system used for the measurement. Reproduced with permission from Hoffmann *et al.*, APL Mater. **8**, 031110 (2020). Copyright 2020 AIP Publishing. (b) Arrhenius plot of the SiO signals collected in vacuum (black squares) for the experimental determination of the activation energy in comparison with the extrapolated activation energy from theory[27] (red and black lines, respectively).

corresponding Φ_{SiO} for $T_{SiO} = 1000\,°C$ ($\Phi_{SiO}^{1000\,°C} = 4.8 \times 10^{13}\,cm^{-2}\,s^{-1}$) toward lower T_{SiO} by

$$\Phi_{SiO}(T) = \Phi_{SiO}^{1000\,°C}\, e^{[-E_a(1/kT - 1/k1000\,°C)]}, \qquad (1)$$

with Boltzmann's constant k, activation energy E_a from the QMS experiment [red line in Fig. 1(b)], and $\Phi_{SiO}^{1000\,°C}$ extracted from the growth rate of an amorphous SiO_2 layer as described in the supplementary material. The extrapolation described in Eq. (1) is shown as

the solid line in Fig. 3. Knowing the β-Ga_2O_3 growth rate—in our case, a typical value is $GR_{Ga2O3} = 4.5\,nm/min$—it is possible to derive the expected Si doping concentration, e.g., $N_{Si} = 6.4 \times 10^{21}\,cm^{-3}$ for $T_{SiO} = 1000\,°C$ using
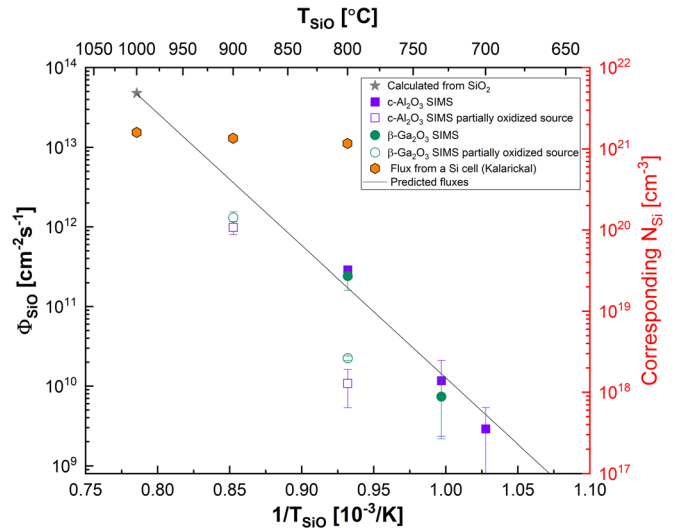
FIG. 3. SiO flux at the substrate as a function of T_{SiO}; the right red scale shows the corresponding doping concentration N_{Si} considering a fixed β-Ga_2O_3 GR = 4.5 nm/min. Empty points refer to layers grown with a partially oxidized source. For the filled ones, the SiO cell was ramped up to $T_{SiO} = 1100\,°C$ before the deposition (dwell t = 30 min) in order to restore the SiO source before the growth. The error bars represent the variation in the doping concentration along the layer thickness with respect to its average concentration. The solid black line refers to the extrapolated SiO flux calculated using Eq. (1). Literature data[13] (orange filled hexagons) for the flux from an elemental Si source during PAMBE growth are reported as a comparison.
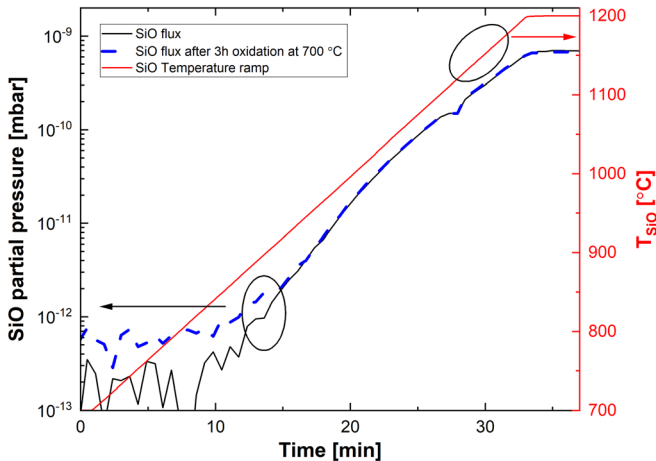

FIG. 2. Partial pressure from the SiO source for a ramp from 400 to 1200 °C before oxidation (black solid line) and after 3 h with molecular oxygen background p = 10^{-5} mbar at $T_{SiO} = 700\,°C$ (blue dashed line). After the 3 h at p = 10^{-5} mbar, the O-flow was closed and the chamber was pumped down to p = 5×10^{-8} mbar in 5 min. The source was then ramped up at 1200 °C.

$$N_{Si} = \frac{\Phi_{SiO}(T)}{GR_{Ga_2O_3}}. \qquad (2)$$

The predicted values obtained from Eqs. (1) and (2) were used as our guideline to investigate different doping concentrations in β-Ga_2O_3 layers on both $Al_2O_3(0001)$ and β-$Ga_2O_3(010)$ substrates grown at T_g of 550 and 750 °C, respectively (see the supplementary material). Depth profiles of the Si dopant were obtained by time-of-flight secondary ion mass spectrometry (ToF-SIMS IV, iontof GmbH, Germany). For quantification, the relative sensitivity factor for silicon in a gallium oxide matrix was obtained by measuring an implantation standard of Si into a nominally undoped β-Ga_2O_3 single crystal with a 10^{14} cm^{-2} fluence and an implantation energy of 80 keV.

In Fig. 3, symbols represent the different ϕ_{SiO} at the substrate as function of the corresponding T_{SiO}, calculated as the product of N_{Si} (measured by SIMS) and $GR_{Ga_2O_3}$ (obtained from SIMS profile) following Eq. (2). For reference, the corresponding volumetric Si concentrations are shown assuming a fixed growth rate of 4.5 nm/min (average GR of the deposited samples) on the right y-scale of Fig. 3. The obtained broad range of Si doping concentrations from 3–4×10^{17} cm^{-3} (T_{SiO} = 700 °C) up to 1.7×10^{20} cm^{-3} (T_{SiO} = 900 °C) demonstrates the possibility to use a SiO source charge for continuous doping in β-Ga_2O_3 thin films controlled by the source temperature in PAMBE. Nonetheless, it was not possible to demonstrate the possibility of achieving doping concentrations below 3×10^{17} cm^{-3} due to an unintentional Si incorporation in the nominally undoped β-Ga_2O_3 layers of around $N_{Si} = 2 \times 10^{17}$ cm^{-3} detected by SIMS. We tentatively relate this unintentional Si incorporation to the plasma source as recently pointed out by Asel et al.[24]

A close inspection of the Si doping profiles of all the deposited β-Ga_2O_3 films reveals a systematically decreasing Si concentration toward the surface, as exemplarily shown in Fig. 4(a). The respective highest and lowest Si concentrations from the begin and end of the doped layers are reflected by the corresponding error bars in Fig. 3. Before the growth of the doped layers, the SiO cell was kept at the corresponding temperature for 15–60 min, in order to exclude the thermalization of the source as the possible origin of the slope. Consequently, we attribute the decreasing Si concentration in the doping profiles to progressive oxidation of the surface of the source material into SiO_2 during PAMBE growth. This finding is just apparently in contrast to the absence of source oxidation in molecular oxygen (see Fig. 2), since it confirms the findings of Kalarickal et al.[13] who suggested active oxygen to play a major role for the oxidation of the Si source into SiO_2 in PAMBE. To further understand the impact of source oxidation, two different data sets are provided in Fig. 3. The empty symbols mark samples grown with a partially oxidized source, while the filled ones show data for samples where a high temperature cycle (T_{SiO} = 1100 °C, t = 30–60 min) was carried out before the layer growth to degas and restore the SiO surface. At T_{SiO} = 800 °C, the comparison between the two sets of data leads to a difference around 1.5 orders of magnitude for the Φ_{SiO} (cf. Fig. 3). Notwithstanding, the Si concentrations from the begin of the layers grown with a freshly degassed cell (upper error bar of filled symbols in Fig. 3) follow the vapor pressure behavior of SiO, confirming the principal control of Si-doping by the source temperature rather than the background pressure. Doping values from the literature[13] concerning Si doping using an elemental Si source inside a PAMBE system are

also reported in Fig. 3 (filled orange hexagons); the comparison with the experimental data collected in this work permits to highlight the significantly increased control of a SiO-source compared to a Si one. In addition, the matching incorporated SiO-flux concentration at the same T_{SiO} both on (0001) Al_2O_3 (T_g = 550 °C) and β-Ga_2O_3 (T_g = 750 °C) suggests (i) a negligible dependence of Si-incorporation on the T_g as was instead observed for Ge[14] and (ii) a negligible dependence on the β-Ga_2O_3 growth orientation [i.e., (−201) and (010), respectively].

Further inspection of Fig. 4(a) suggests the slope of the decreasing Si-concentration to depend on the SiO cell temperature, being steeper for a T_{SiO} = 700 °C compared to the one at 800 °C. In a simple oxidation model [pictorially explained in Fig. 4(c)], the unoxidized area of the source material (that can provide a SiO flux) decreases with a decay constant λ. Considering a fixed probability per unit time that a certain percentage of the SiO source surface will further oxidize into SiO_2, as a function of T_{SiO} and the oxygen background pressure in the MBE chamber, we expect an exponential decay of the accessible SiO surface, and hereby of the SiO flux. Consequently, an exponentially decreasing Φ_{SiO} (which is proportional to this area) is expected during source oxidation,

$$\Phi_{SiO}(t) = \Phi_{SiO}(0)e^{-\lambda \cdot t}, \qquad (3)$$

where $\Phi_{SiO}(0)$ corresponds to the flux at $t = 0$. Using Eq. (3), Eq. (2), and the relation between layer thickness d and corresponding growth time t ($d = GR_{Ga_2O_3}t$), we extracted λ from the slopes of the SIMS profiles $d(\ln N_{Si})/d(d)$ as

$$\lambda = GR_{Ga_2O_3}d(\ln N_{Si})/d(d). \qquad (4)$$

Figure 4(b) shows the extracted λ for layers doped at different T_{SiO} and suggests two different regimes: (i) for $T_{SiO} > 730$ °C, almost flat doping profiles signify a low decay constant, (ii) for lower T_{SiO}, a high λ indicates non-stable doping throughout the layer thickness (e.g., decrease in the doping concentration from 6.8×10^{17} cm^{-3} down to 2×10^{17} cm^{-3} in a deposition time $t = 15$ min, i.e., over a 90 nm layer thickness). These data suggest lower T_{SiO} (within the investigated range) to promote oxidation of the source, similar to the observations of Kim et al. for the Sr source oxidation,[30] and in very good agreement with Kalarickal et al.,[13] that determined passive oxidation of an elemental Si source into SiO_2 at $T_{Si} = 750$ °C and active oxidation into SiO at $T_{Si} \geq 800$ °C during PAMBE growth of Si-doped Ga_2O_3. Hence, the low temperature and, consequentially, low doping regime requires further measures to reduce the oxidation of the source in order to achieve more uniform doping profiles.

In order to understand how the active oxygen in the chamber affects the oxidation of the source, a preliminary study of the decay constant, for a fixed T_{SiO} = 800 °C, as a function of both the oxygen flux and the plasma power [inset Fig. 4(b)] is provided. More data will be needed in order to completely understand and model this behavior but, a reduction of the oxygen flux, from 1 sccm down to 0.33 sccm, clearly shows a significant reduction of the decay constant (around two times less at 400 W at the same T_{SiO}). For the plasma power the data show some inconsistency. In fact, while at the lower flux O_{flux} = 0.33 sccm and low plasma power (150 W), a lower decay constant is found compared to the sample with the same oxygen flux, at higher plasma power (400 W, hence, a larger amount of active oxygen), for
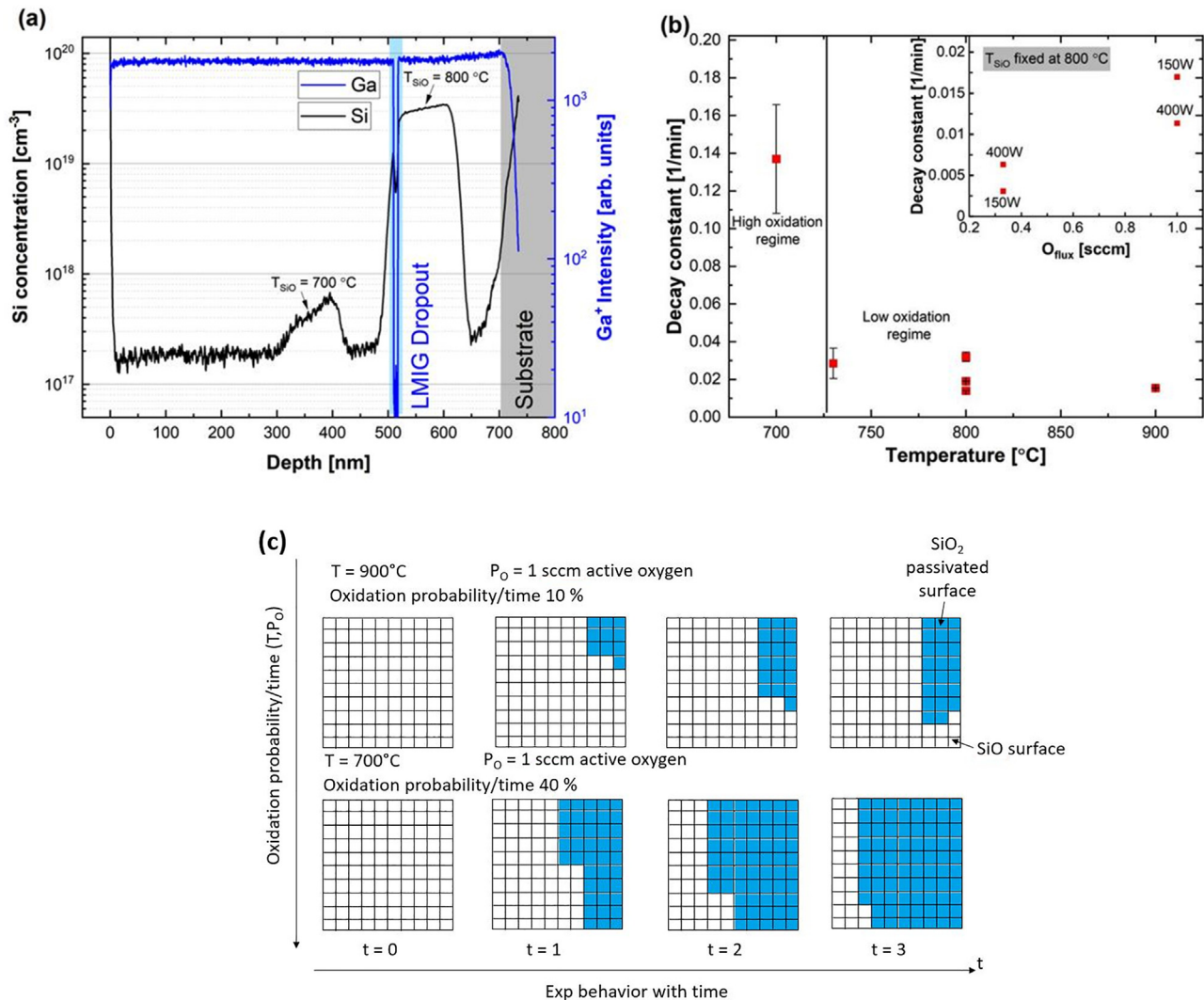
FIG. 4. (a) SIMS doping profile for a β-Ga$_2$O$_3$ sample grown with different T_{SiO}. The drop of the signal around 500 nm is an artifact caused by a dropout of the liquid metal ion gun (LMIG). A slope in the SiO profile is visible, showing a steeper slope at lower T_{SiO}. (b) Decay constant calculated from a linear fit of the SIMS profile in log scale. Before the fitting, the Si background was subtracted and used to calculate the error bar. The error bars highlight how the background subtraction become important, i.e., how close the measured concentration is with respect to the background level (defined for nominally undoped layers). Inset: dependence of the decay constant on the active oxygen in the chamber for a fixed $T_{SiO} = 800\,°C$. (c) Schematics of the oxidation process that may take place on the SiO source as a function of T_{SiO} and active oxygen background pressure. In this case, the active oxygen pressure is fixed.

the higher supplied flux O$_{flux}$ = 1 sccm, the trend is inverted. This unexpected behavior is still not clearly understood, and further experiment is needed in order to address this issue.

Finally, room temperature van der Pauw–Hall measurements (details in the supplementary material) were performed on a homoepitaxially grown sample with a 124 nm-thick Si-doped layer (N_{Si} = 3 $\times 10^{19}$ cm^{-3}). The extracted Hall electron concentration of $n = 3 \times 10^{19}$ cm^{-3} with an electron mobility μ of 25 cm^2/V s and a sheet resistance R_s of 645 Ω/sq confirms effective Si-doping by our approach in line with the provided Φ_{SiO}.

In conclusion, we have demonstrated the potential of a solid SiO source to provide a wide range of SiO fluxes controlled by the source

temperature of a conventional effusion cell. Using this source, SiO fluxes at the substrate ranging from 5.5×10^{13} (T_{SiO} = 1000 °C) to 2.9×10^{9} (T_{SiO} = 700 °C) cm^{-2} s^{-1} were used to grow a SiO$_2$ layer as well as continuously Si doping β-Ga$_2$O$_3$ layers with concentrations ranging from 1.7×10^{20} (T_{SiO} = 900 °C) cm^{-3} to 3×10^{17} (T_{SiO} = 700 °C) cm^{-3} inside an oxide PAMBE. Hall measurements of a homoepitaxial Si-doped β-Ga$_2$O$_3$ layer deposited with a T_{SiO} corresponding to an expected N_{Si} = 3×10^{19} cm^{-3} (800 °C) revealed the same charge carrier density ($n = 3 \times 10^{19}$ cm^{-3}) indicating effective doping. The Si-incorporation was essentially the same for Ga$_2$O$_3$(010) homoepitaxially grown at 750 °C and Ga$_2$O$_3$(−201) heteroepitaxially grown at 550 °C.

An oxidation of the SiO source, leading to a decreasing SiO flux, has been observed in active oxygen (plasma) but not in molecular oxygen at similar background pressures. The decreasing flux has been parametrized by a decay constant λ extracted from the measured Si-doping profiles. Our initial data indicate a strong oxidation regime ($\lambda \geq 0.14\,\mathrm{min}^{-1}$) for relatively low T_{SiO} ($\leq 730\,^\circ\mathrm{C}$) and a milder one ($\lambda < 0.015\,\mathrm{min}^{-1}$) at higher T_{SiO} ($\geq 800\,^\circ\mathrm{C}$) at 250 W. The partial oxidation of the source can be reproducibly reverted by degassing at T_{SiO} = 1100 °C. Reducing the supplied oxygen flux has been shown to reduce the oxidation of the source (lowest recorded $\lambda = 0.003\,\mathrm{min}^{-1}$ at 0.33 sccm and 150 W), while the effect on the plasma power on the oxidation process is still unclear and further experiments will be needed in order to provide a definitive answer.

We believe that our approach can be also applied to O₃-MBE[26] as well as for doping of other oxides, e.g., In₂O₃. Suggested measures to reduce the source oxidation during growth by oxygen PAMBE include (i) an increased T_{SiO} or (ii) a decreased activated oxygen p_{O2} at the SiO source. The (i) can be realized by a modified source geometry, e.g., using an aperture on the crucible[31] or an increased source-to-substrate distance,[30] to necessitate a higher SiO vapor pressure (and thus higher T_{SiO}) inside the crucible to obtain the same SiO flux at the substrate. The (ii) can be realized by the same aperture as in (i), a differentially pumped SiO source,[32] or by using growth conditions that require less oxygen,[33] e.g., metal-exchange catalyzed MBE (MEXCAT-MBE).[34–37]

See the supplementary material for the growth of the amorphous SiO₂ layer that was used in order to calibrate our flux predictions (Fig. 3). Furthermore, details on the growth of the β-Ga₂O₃ layers and additional information on the transport measurements are also provided.

AUTHOR DECLARATIONS
Conflict of Interest

The authors have no conflicts to disclose.

Author Contributions

Andrea Ardenghi: Data curation (equal); Formal analysis (equal); Investigation (equal); Writing – original draft (equal); Writing – review and editing (equal). **Oliver Bierwagen:** Conceptualization (equal); Data curation (equal); Formal analysis (equal); Investigation (equal); Methodology (equal); Project administration (equal); Supervision (equal); Writing – review and editing (equal). **Andreas Falkenstein:** Investigation (equal); Methodology (equal); Writing – review and editing (supporting). **Georg Hoffmann:** Investigation (supporting); Writing – review and editing (supporting). **Jonas Lähnemann:** Investigation (supporting); Writing – review and editing (supporting). **Manfred Martin:** Investigation (supporting); Methodology (supporting); Writing – review and editing (supporting). **Piero Mazzolini:** Conceptualization (lead); Data curation (equal); Formal analysis (equal); Funding acquisition (lead); Investigation (equal); Project administration (lead); Supervision (lead); Writing – original draft (equal); Writing – review and editing (equal).

DATA AVAILABILITY

The data that support the findings of this study are available from the corresponding authors upon reasonable request.

REFERENCES

[1] X. Yu, T. J. Marks, and A. Facchetti, Nat. Mater. **15**, 383 (2016).

[2] S. J. Pearton, J. Yang, P. H. Cary, F. Ren, J. Kim, M. J. Tadjer, and M. A. Mastro, Appl. Phys. Rev. **5**, 011301 (2018).

[3] M. Higashiwaki, K. Sasaki, A. Kuramata, T. Masui, and S. Yamakoshi, Appl. Phys. Lett. **100**, 013504 (2012).

[4] Z. Galazka, R. Uecker, D. Klimm, K. Irmscher, M. Naumann, M. Pietsch, A. Kwasniewski, R. Bertram, S. Ganschow, and M. Bickermann, ECS J. Solid State Sci. Technol. **6**, Q3007 (2017).

[5] A. Kuramata, K. Koshi, S. Watanabe, Y. Yamaoka, T. Masui, and S. Yamakoshi, Jpn. J. Appl. Phys., Part 1 **55**, 1202A2 (2016).

[6] E. Ohba, T. Kobayashi, T. Taishi, and K. Hoshikawa, J. Cryst. Growth **556**, 125990 (2021).

[7] E. G. Villora, K. Shimamura, Y. Yoshikawa, K. Aoki, and N. Ichinose, J. Cryst. Growth **270**, 420 (2004).

[8] A. J. Green, J. Speck, G. Xing, P. Moens, F. Allerstam, K. Gumaelius, T. Neyer, A. Arias-Purdue, V. Mehrotra, A. Kuramata, K. Sasaki, S. Watanabe, K. Koshi, J. Blevins, O. Bierwagen, S. Krishnamoorthy, K. Leedy, A. R. Arehart, A. T. Neal, S. Mou, S. A. Ringel, A. Kumar, A. Sharma, K. Ghosh, U. Singisetti, W. Li, K. Chabak, K. Liddy, A. Islam, S. Rajan, S. Graham, S. Choi, Z. Cheng, and M. Higashiwaki, APL Mater. **10**, 029201 (2022).

[9] A. Kyrtsos, M. Matsubara, and E. Bellotti, Appl. Phys. Lett. **112**, 032108 (2018).

[10] E. Ahmadi, O. S. Koksaldi, X. Zheng, T. Mates, Y. Oshima, U. K. Mishra, and J. S. Speck, Appl. Phys. Express **10**, 071101 (2017).

[11] A. Mauze, Y. Zhang, T. Itoh, F. Wu, and J. S. Speck, APL Mater. **8**, 021104 (2020).

[12] A. Mauze, Y. Zhang, T. Itoh, E. Ahmadi, and J. S. Speck, Appl. Phys. Lett. **117**, 222102 (2020).

[13] N. K. Kalarickal, Z. Xia, J. McGlone, S. Krishnamoorthy, W. Moore, M. Brenner, A. R. Arehart, S. A. Ringel, and S. Rajan, Appl. Phys. Lett. **115**, 152106 (2019).

[14] E. Ahmadi, O. S. Koksaldi, S. W. Kaun, Y. Oshima, D. B. Short, U. K. Mishra, and J. S. Speck, Appl. Phys. Express **10**, 041102 (2017).

[15] S. Krishnamoorthy, Z. Xia, S. Bajaj, M. Brenner, and S. Rajan, Appl. Phys. Express **10**, 051102 (2017).

[16] Z. Feng, A. F. M. Anhar Uddin Bhuiyan, M. R. Karim, and H. Zhao, Appl. Phys. Lett. **114**, 250601 (2019).

[17] X. Du, Z. Li, C. Luan, W. Wang, M. Wang, X. Feng, H. Xiao, and J. Ma, J. Mater. Sci. **50**, 3252 (2015).

[18] F. Alema, G. Seryogin, A. Osinsky, and A. Osinsky, APL Mater. **9**, 091102 (2021).

[19] A. Hernandez, M. M. Islam, P. Saddatkia, C. Codding, P. Dulal, S. Agarwal, A. Janover, S. Novak, M. Huang, T. Dang, M. Snure, and F. A. Selim, Results Phys. **25**, 104167 (2021).

[20] M. Baldini, M. Albrecht, A. Fiedler, K. Irmscher, R. Schewski, and G. Wagner, ECS J. Solid State Sci. Technol. **6**, Q3040 (2017).

[21] S. Bin Anooz, R. Grüneberg, T.-S. Chou, A. Fiedler, K. Irmscher, C. Wouters, R. Schewski, M. Albrecht, Z. Galazka, W. Miller, J. Schwarzkopf, and A. Popp, J. Phys. D **54**, 034003 (2021).

[22] S. Lany, APL Mater. **6**, 046103 (2018).

[23] T. Kamimura, Y. Nakata, M. H. Wong, and M. Higashiwaki, IEEE Electron Device Lett. **40**, 1064 (2019).

[24] T. J. Asel, E. Steinbrunner, J. Hendricks, A. T. Neal, and S. Mou, J. Vac. Sci. Technol., A **38**, 043403 (2020).

[25] G. Hoffmann, Z. Cheng, O. Brandt, and O. Bierwagen, APL Mater. **9**, 111110 (2021).

[26]M. Higashiwaki, K. Sasaki, A. Kuramata, T. Masui, and S. Yamakoshi, Phys. Status Solidi A **211**, 21 (2014).

[27]K. M. Adkison, S.-L. Shang, B. J. Bocklund, D. Klimm, D. G. Schlom, and Z.-K. Liu, APL Mater. **8**, 081110 (2020).

[28]G. Hoffmann, M. Budde, P. Mazzolini, and O. Bierwagen, APL Mater. **8**, 031110 (2020).

[29]P. Vogt, F. V. E. Hensling, K. Azizie, C. S. Chang, D. Turner, J. Park, J. P. McCandless, H. Paik, B. J. Bocklund, G. Hoffman, O. Bierwagen, D. Jena, H. G. Xing, S. Mou, D. A. Muller, S.-L. Shang, Z.-K. Liu, and D. G. Schlom, APL Mater. **9**, 031101 (2021).

[30]Y. S. Kim, N. Bansal, C. Chaparro, H. Gross, and S. Oh, J. Vac. Sci. Technol., A **28**, 271 (2010).

[31]Y.-S. Kim, N. Bansal, and S. Oh, J. Vac. Sci. Technol., A **28**, 600 (2010).

[32]Y.-S. Kim, N. Bansal, and S. Oh, J. Vac. Sci. Technol., A **29**, 041505 (2011).

[33]P. Mazzolini and O. Bierwagen, J. Phys. D **53**, 354003 (2020).

[34]P. Mazzolini, A. Falkenstein, C. Wouters, R. Schewski, T. Markurt, Z. Galazka, M. Martin, M. Albrecht, and O. Bierwagen, APL Mater. **8**, 011107 (2020).

[35]P. Vogt, O. Brandt, H. Riechert, J. Lähnemann, and O. Bierwagen, Phys. Rev. Lett. **119**, 196001 (2017).

[36]P. Mazzolini, P. Vogt, R. Schewski, C. Wouters, M. Albrecht, and O. Bierwagen, APL Mater. **7**, 022511 (2019).

[37]P. Mazzolini, A. Falkenstein, Z. Galazka, M. Martin, and O. Bierwagen, Appl. Phys. Lett. **117**, 222105 (2020).